Electronic structure and molecular properties of the octacyanorhenate $[Re(CN)_8]^{3-}$ and $[Re(CN)_8]^{2-}$ complexes

Jorge David [a], Fernando Mendizábal [b], Ramiro Arratia-Pérez [a,*]

[a] *Departamento de Ciencias Químicas, Universidad Andrés Bello, República 275, Santiago, Chile*
[b] *Departamento de Química, Facultad de Ciencias, Universidad de Chile, Casilla 653, Santiago, Chile*

Abstract

We report scalar and four component relativistic density functional calculations on octacyanorhenate $[Re(CN)_8]^{2-}$ and $[Re(CN)_8]^{3-}$ complexes. The relativistic calculations predict that the molecular *g*-tensor of the paramagnetic $[Re(CN)_8]^{2-}$ complex is isotropic. The calculated optical electronic transitions for both complexes with a polarizable continuum model using a time dependent density functional (TDDFT)/B3LYP formalism suggest that the $[Re(CN)_8]^{3-}$ complex may distort towards dodecahedral geometry in solution. The electronic excitations of LMCT type of $[Re(CN)_8]^{2-}$ are displaced at very high wavelengths with significant oscillator strength values which is characteristic of Re compounds having luminescent behaviour. Thus, our calculations predict that $[Re(CN)_8]^{2-}$ could be luminescent.

1. Introduction

In recent years there has been great interest in the chemistry and properties of metal–cyanide complexes and clusters due to their possible use for an assortment of applications that include electronics, magnetism and catalysis [1–3]. Thus, the title metal–cyanide complexes are viewed as useful molecular precursors, which can be, incorporated into high-nuclearity clusters with adjustable magnetic properties and could be of utility in the design of cyano-bridged materials with potentially technological applications [1,4,5]. It is expected that the incorporation of third-row transition metal complexes may enhance the utility of such materials since these third-row transition metals possess higher-energy valence d orbitals that may induce interesting magnetic properties due to the effects of significant spin–orbit coupling [3–5].

In particular, the low-spin (d^2) $[Re(CN)_8]^{3-}$ complex have been structurally characterized [5]. The X-ray analysis of single crystals of the $[Re(CN)_8]^{3-}$ salt has indicated that adopt the square antiprismatic (D_{4d}) geometry, while the paramagnetic (d^1) $[Re(CN)_8]^{2-}$ complex has been postulated as the photo-oxidized product of $[Re(CN)_8]^{3-}$ [5]. The electronic structure and spectral assignments of the octacyanide rhenium complexes were discussed in 1963 by Perumareddi et al. [6] and Griffith et al. [7] using ligand field theory, and no other studies on these complexes are currently known. However, recent ab initio CASSCF and CASPT2 calculations for the assignment of the electronic spectra of the (d^2) $[Mo(CN)_8]^{4-}$, $[W(CN)_8]^{4-}$, and (d^1) $[Mo(CN)_8]^{3-}$ complexes have been reported by Hendrickx et al. [8,9].

In view of the current interest in metal–cyanide materials, we have investigated in this Letter, the electronic structure and spectral properties of above mentioned rhenium–octacyanide complexes using scalar and four component relativistic (DSW) calculations with the purpose of identifying relativistic and electron correlation effects on the ground and excited states properties of both complexes. We also performed time-dependent density functional (TDDFT) calculations including solvent effects to rationalize their optical spectra, ZORA [13] and DSW first-order perturbational calculations to estimate the molecular *g*-tensor of the (d^1) $[Re(CN)_8]^{2-}$ complex.

* Corresponding author.
E-mail addresses: j.david@uandresbello.edu (J. David), hagua@uchile.cl (F. Mendizábal), rarratia@unab.cl (R. Arratia-Pérez).

2. Details of the calculations

The geometry optimizations of each complex in a vacuum were carried out using the Amsterdam density functional code (ADF) [10] developed by Baerends and co-workers [11–13]. Electron correlation was treated within the LDA approximation, and non-local Becke exchange [14] and Perdew correlation gradient corrections [15,16] were included in the calculations. Solvation effects were estimated in a polarized continuum model (PCM) [17–19] of acetonitrile solutions using the GAUSSIAN98 package [20] with the B3LYP functional, where for Re the 15 valence electrons quasirelativistic pseudopotentials of Andrae et al. [21] was employed, while for the C and N atoms, pseudopotentials using double-ξ basis sets with the addition of one d-type polarization function were employed [22]. The calculation of the excitation energies of each complex in a PCM were done at the B3LYP level using the time-dependent perturbation density functional theory approach (TDDFT) [23,24]. The TDDFT approach provides an alternative to computationally demanding multireference configuration interaction methods for the calculation of excitation energies [24].

We also performed Dirac scattered wave (DSW) calculations to estimate spin–orbit effects and spin-dependent properties. In this formalism, an effective Coulomb and exchange-correlation potential approximate the Dirac four-component wave function as a Slater determinant. [25,26,28–30]. The exchange-correlation potential is modeled by a relativistic local density potential according to MacDonald and Vosko [31,32]. For the calculation of the Zeeman magnetic splittings we start with a Dirac self-consistent four-component wave function Φ and we employ a first-order perturbation procedure. The effects of an external magnetic field is described by a relativistic perturbation Hamiltonian $H_1 = e\boldsymbol{\alpha}\cdot\mathbf{A}$, where $\boldsymbol{\alpha}$ is the 4×4 Dirac matrix composed of zeros on the diagonal, and the Pauli spin matrices in the off-diagonal positions, and, $\mathbf{A}$ is the electromagnetic four-vector potential. When the magnetic nuclei is in the presence of an external magnetic field $\mathbf{B}$, this four-vector potential is represented by $\mathbf{A} = 1/2(\mathbf{B}\times\mathbf{r})$, and, the Zeeman magnetic interactions are then described by the perturbation Hamiltonian $H_Z = 1/2e\boldsymbol{\alpha}\cdot(\mathbf{B}\times\mathbf{r})$ [28–30,33].

Table 1
Group relationships between the D_{4d} and D^*_{4d} point groups

Direct product for the D^*_{4d} double point group

D^*_{4d}	Γ_8	Γ_9	Γ_{10}	Γ_{11}
Γ_8	$A_1 + A_2 + E_3$	$E_1 + E_2$	$B_1 + B_2 + E_1$	$E_2 + E_3$
Γ_9		$A_1 + A_2$	$E_2 + E_3$	$B_1 + B_2 + E_3$
Γ_{10}			$A_1 + A_2 + E_3$	$E_1 + E_2$
Γ_{11}				$A_1 + A_2 + E_1$

Compatibility table between $D_{4d} \rightarrow D^*_{4d}$

	A_1	A_2	B_1	B_2	E_1	E_2	E_3
Γ_8	Γ_8	Γ_8	Γ_{10}	Γ_{10}	$\Gamma_9 + \Gamma_{10}$	$\Gamma_9 + \Gamma_{11}$	$\Gamma_8 + \Gamma_{11}$

The $\langle\Phi|H_1|\Phi\rangle$ matrix elements are evaluated in the basis spanning the 'two' rows of the double valued irreducible representations of the paramagnetic complex holding the single electron spin. Since the $\boldsymbol{\alpha}$ matrices are off-diagonal, the evaluation of the matrix elements involves products of the 'large' and 'small' components of the Dirac wavefunction. The resulting perturbation energies are then fitted to the usual spin Hamiltonian $H_{spin} = \mathbf{S}\cdot\mathbf{g}\cdot\mathbf{B}$, where a convenient parameterized value of $\mathbf{S} = 1/2$ is used to describe the ground state Kramers doublet, being $\mathbf{g}$ its associated g-tensor [28,29,33,34].

To facilitate the analysis and understanding of our scalar relativistic and Dirac scattered-wave calculations, we provide in Table 1 the group relationships between the single (D_{4d}) and double (D^*_{4d}) point groups.

3. Results and discussion

The results of the geometry optimization performed in a vacuum and in a polarized continuum of acetonitrile solutions (PCM) [17–19], are listed in Table 2. It can be seen from Table 2 that the removal of one electron in $[Re(CN)_8]^{3-}$ does not induce severe alterations in their geometries. Although, no structural data are yet available for the paramagnetic $[Re(CN)_8]^{2-}$ ion, its existence is extracted from the cyclic voltammogram in acetonitrile which indicates that $[Re(CN)_8]^{3-}$ oxidizes to $[Re(CN)_8]^{2-}$ at $E_{1/2} = 0.999$ V vs. $Cp_2Fe^{0/1+}$ [5]. The computed bond distances and bond angles, in both phases, are in reasonable agreement with the averaged experimental values of $[Re(CN)_8]^{3-}$ [5].

Table 2
Bond lengths (Å) and angles (°) of the $[Re(CN)_8]^{2-}$ and $[Re(CN)_8]^{3-}$ anions

	$[Re(CN)_8]^{2-}$		$[Re(CN)_8]^{3-}$		
	Calc.[a]	Calc.[b]	Calc.[a]	Calc.[b]	Expt.[c]
Distances					
Re–C	2.09	2.15	2.11	2.15	2.09
C–N	1.17	1.16	1.16	1.15	1.16
Angles					
C–Re–C	78.9, 113.5, 142.7	72.1, 112.7, 142.8	79.3, 112.9, 142.8	75.5, 113.5, 142.7	76.0, 114.3, 142.5
Re–C–N	178.3	180.0	177.5	180.0	177.7

[a] Gas-phase optimization with ADF method.
[b] Optimization in acetonitrile solutions with GAUSSIAN98+B3LYP.
[c] X-ray structure of $K_3[Re(CN)_8]\cdot 2MeCN$, see Ref. [5].

3.1. Molecular orbitals

The ligands and metal interact through charge transfers among the 4σ, 5σ, 1π, and $2\pi^*$ ligand cyanide orbitals, and the rhenium s, p, and d orbitals. The metal–ligand bonding interactions are mainly governed by the usual mechanism of σ donation by the cyanide being accompanied by $2\pi^*$ back-donation from the rhenium d_{z^2} orbitals. Table 3 shows the total valence populations for both complexes given in terms of atomic spinors. It can be seen from this table that the rhenium 5d occupation is substantially larger than the value of 1 and 2 predicted by the d^1 and d^2 crystal field models. The same result is obtained from the scalar ADF calculations. This in line with net charge transfers of ~0.6e and ~0.5e per ligand molecule donated to the rhenium 5d orbitals, which form the metal–ligand bond. It is also possible to extract from Table 3 the ratios of occupied character for the $j = \ell - 1/2$ and $j = \ell + 1/2$ sublevels. In the nonrelativistic limit these ratios are required by symmetry to be $(\ell + 1)/\ell$, for $\ell > 0$. For d orbitals this nonrelativistic ratio is 1.50. The values of 1.34 and 1.33 obtained from Table 3 for the rhenium valence 5d orbitals indicates that the $d_{3/2}$ orbitals are clearly favored over $d_{5/2}$, as expected for a relatively large spin–orbit coupling constant.

The calculated energy gaps between the occupied and unoccupied states of both complexes are large (~4.0 eV), so that it is a good approximation to represent their ground states as a single determinant. Under a square antiprismatic (D_{4d}) crystal field the rhenium d-orbitals split (and are populated) in $[Re(CN)_8]^{3-}$ according to $(da_1)^{1.76}$ $(de_2)^{2.17}$ $(de_3)^{1.94}$ as calculated by the ADF code, while, the calculation by the DSW code gives $(da_1)^{1.87}$ $(de_2)^{2.14}$ $(de_3)^{1.98}$, respectively. Similarly, the d-splitting and populations in $[Re(CN)_8]^{2-}$ are $(da_1)^{1.29}$ $(de_2)^{2.26}$ $(de_3)^{2.11}$ as calculated by the ADF code, while, the calculation by the DSW code gives $(da_1)^{1.44}$ $(de_2)^{2.18}$ $(de_3)^{2.13}$, respectively. It can be inferred from Table 1 that de_2 transform as $d(\gamma_9 + \gamma_{11})$, de_3 as $d(\gamma_8 + \gamma_{11})$ and da_1 as $d\gamma_8$.

The HOMO of each component of the $[Re(CN)_8]^{2-/3-}$ redox couple span the a_1 symmetry representation, and, in both cases arises primarily (~60%) from the metal ($5d_{z^2}$) and the rest arises from nitrogens (~28%) and carbons (~10%). The LUMO span the e_2 representation which splits

Table 3
Total valence populations (electrons/atom)

Atom	ℓ	j	$[Re(CN)_8]^{2-}$	$[Re(CN)_8]^{3-}$
Re	0	1/2	0.616	0.603
	1	1/2	0.322	0.313
	1	3/2	0.506	0.501
	2	3/2	2.460	2.561
	2	5/2	3.297	3.429
Total Re			7.201	7.407
C	0	1/2	1.156	1.178
	1	1/2	0.956	0.955
	1	3/2	1.899	1.901
Total C			4.011	4.034
N	0	1/2	1.374	1.369
	1	1/2	1.281	1.308
	1	3/2	2.560	2.614
Total N			5.215	5.291

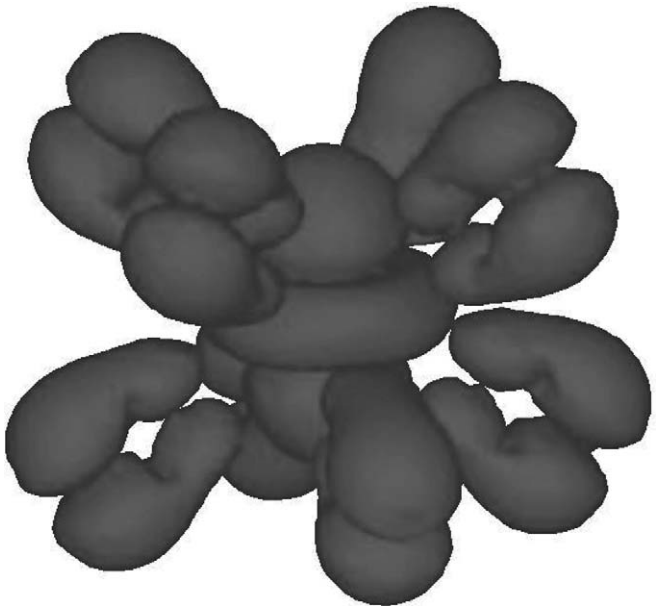

Fig. 1. Relativistic three-dimensional (3D) spin density plot (electron/$bohr^3)^{3/2}$ of the $[Re(CN)_8]^{2-}$ complex.

Table 4
TD-DFT/B3LYP singlet-excitation calculations for $[Re(CN)_8]^{3-}$ and $[Re(CN)_8]^{2-}$ in MeCN solution phase (PCM)

λ_{calc} (nm)	f [a]	λ_{exp} (nm)[b]	Contributions[c]	Type transition
A. $[Re(CN)_8]^{3-}$				
356.9	0.0	348	$45A_1 \rightarrow 46E_2$ (94.1)	MMCT ($d_{z^2} \rightarrow d_{xy}$)
			$45A_1 \rightarrow 47E_2$ (94.1)	MMCT ($d_{z^2} \rightarrow d_{x^2-y^2}$)
302.7	0.0	298	$45A_1 \rightarrow 48E_3$ (94.8)	MMCT ($d_{z^2} \rightarrow d_{xz}$)
			$45A_1 \rightarrow 48E_3$ (94.8)	MMCT ($d_{z^2} \rightarrow d_{yz}$)
244.2	0.0	252	$45A_1 \rightarrow 50E_3$ (98.2)	MMCT ($d_{z^2} \rightarrow d_{yz}$)
212.1	0.0234	231	$45A_1 \rightarrow 51E_1$ (61.6)	MMCT ($d_{z^2} \rightarrow p_x$)
			$45A_1 \rightarrow 52E_1$ (36.8)	MMCT ($d_{z^2} \rightarrow p_y$)
206.3	0.0042		$36E_2 \rightarrow 47E_2$ (12.0)	LMCT ($\pi \rightarrow d_{xy}$)
			$37E_2 \rightarrow 46E_2$ (12.1)	LMCT ($\pi \rightarrow d_{x^2-y^2}$)
			$45A_1 \rightarrow 53B_2$ (74.4)	MMCT ($d_{z^2} \rightarrow p_z$)
202.9	0.0350	196	$36E_2 \rightarrow 47E_2$ (27.9)	LMCT ($\pi \rightarrow d_{xy}$)
			$37E_2 \rightarrow 46E_2$ (43.8)	LMCT ($\pi \rightarrow d_{x^2-y^2}$)
			$45A_1 \rightarrow 53B_2$ (22.8)	MMCT ($d_{z^2} \rightarrow p_z$)

λ_{calc} (nm)	f [a]	Contributions[c]	Type transition
B. $[Re(CN)_8]^{2-}$			
708.7	0.0022	$42E_1\beta \rightarrow 45A_1\beta$ (100)	LMCT ($\pi^* \rightarrow d_{z^2}$)
708.7	0.0022	$43E_1\beta \rightarrow 45A_1\beta$ (100)	LMCT ($\pi^* \rightarrow d_{z^2}$)
644.4	0.0228	$41B_2\beta \rightarrow 45A_1\beta$ (97.9)	LMCT ($\pi^* \rightarrow d_{z^2}$)
427.9	0.0373	$30E_1\beta \rightarrow 45A_1\beta$ (97.2)	LMCT ($\pi \rightarrow d_{z^2}$)
427.9	0.0373	$31E_1\beta \rightarrow 45A_1\beta$ (97.2)	LMCT ($\pi \rightarrow d_{z^2}$)
382.9	0.0109	$29E_1\beta \rightarrow 45A_1\beta$ (99.0)	LMCT ($\sigma^* \rightarrow d_{z^2}$)
382.9	0.0109	$28E_1\beta \rightarrow 45A_1\beta$ (99.0)	LMCT ($\sigma^* \rightarrow d_{z^2}$)
380.9	0.0172	$27B_2\beta \rightarrow 45A_1\beta$ (99.1)	LMCT ($\sigma^* \rightarrow d_{z^2}$)

[a] Oscillator strength.
[b] See Ref. [5].

by spin–orbit coupling into $(\gamma_9 + \gamma_{11})$ by 0.50 eV ($\sim$4032 cm^{-1}) due to about 40% metal ($5d_{xy}$, $5d_{x^2-y^2}$) content, in both complexes. Thus, according to our calculations the $[Re(CN)_8]^{2-}$ ion is paramagnetic characterized by a Kramer doublet of γ_8 symmetry, while the $[Re(CN)_8]^{3-}$ ion is diamagnetic characterized by a singlet ground state.

The calculated molecular electronegativities [27] (χ) of the paramagnetic $[Re(CN)_8]^{2-}$ ($\chi = 10.3$ eV) and of the diamagnetic $[Re(CN)_8]^{3-}$ ($\chi = 5.9$ eV) complexes suggest that $[Re(CN)_8]^{3-}$ is more reactive than $[Re(CN)_8]^{2-}$. Considering that χ measures the escaping tendency of the electron cloud, the calculated χ indicates that the closed shell complex is more reactive than the open-shell complex. $[Re(CN)_8]^{3-}$ is photoactive upon exposure to UV radiation, presumably oxidizing to the $[Re(CN)_8]^{2-}$ specie [5]. Also, the cyclic voltammogram of $(Bu_4N)_3[Re(CN)_8]$ in acetonitrile displays a quasireversible $[Re(CN)_8]^{3-/2-}$ redox couple centered at $E_{1/2} = 0.99$ V vs. $Cp_2Fe^{0/1+}$ [5].

3.2. Electron spin distribution and molecular g-tensor of $[Re(CN)_8]^{2-}$

In the case of the paramagnetic $[Re(CN)_8]^{2-}$ complex, a unit electron spin distribution should obey the following: $\rho(Re) + 8\rho(C) + 8\rho(N) = 1.000$ [34]. According to our calculations we obtained the following electron spin distribution: $\rho(Re) = 0.592$, $\rho(C) = 0.012$, $\rho(N) = 0.039$. Thus, our relativistic calculations indicate that the single electron spin of the paramagnetic complex is mostly associated to the rhenium $5d_{z^2}$ orbital and nitrogen $2p_z$ orbitals. This can be visualized from Fig. 1, where we show the relativistic three-dimensional (3D) spin density plot of the $[Re(CN)_8]^{2-}$ complex.

The four component DSW and scalar relativistic (ZORA) calculations of the molecular g-tensor of the $[Re(CN)_8]^{2-}$ complex predict an isotropic g-tensor with g values of 1.7324 and 1.6618, respectively. The large negative deviation from the spin-only value of $g_e = 2.0023$ could be explained as arising from the proximity of the LUMO that split by spin–orbit interaction by 0.5 eV due to the $\sim$40% ($5de_2$) Re content. Also, the HOMO-1 (e_1) level split due to spin–orbit interaction by 0.05 eV due to a small ($\sim$4%) Rhenium content.

3.3. Optical properties

The excitation energies were obtained at the B3LYP level from a single point calculations of the D_{4d} models

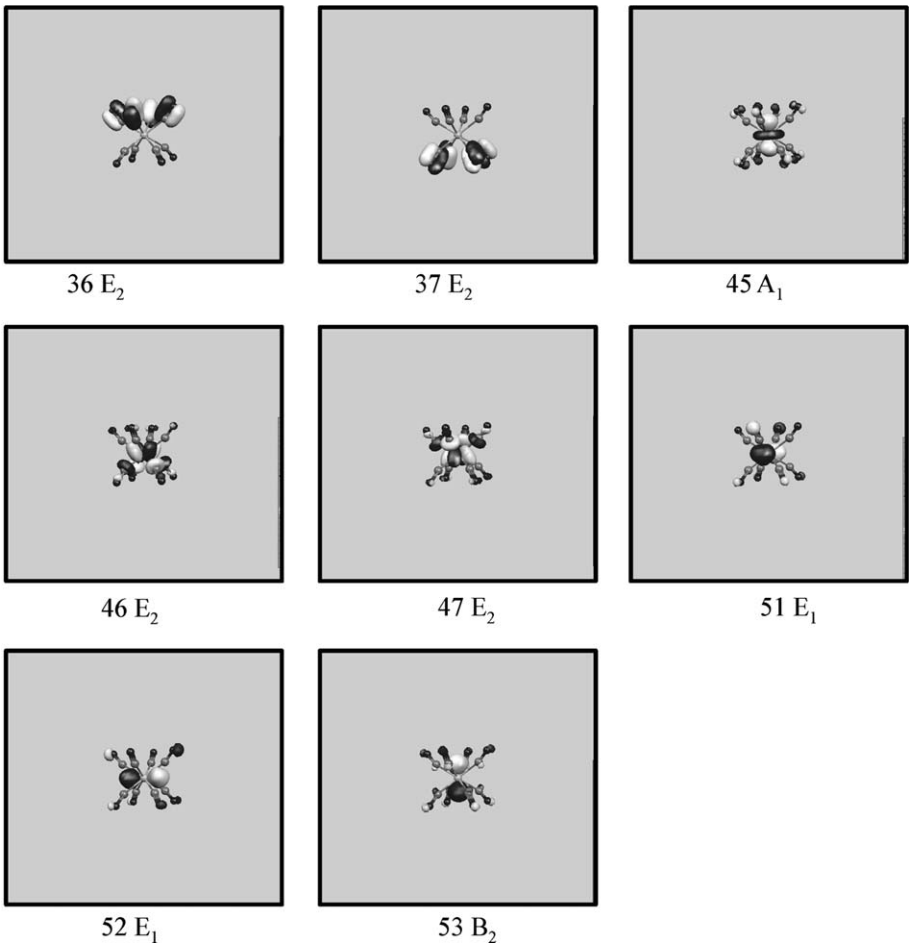

Fig. 2. Active molecular orbitals of the $[Re(CN)_8]^{3-}$ complex.

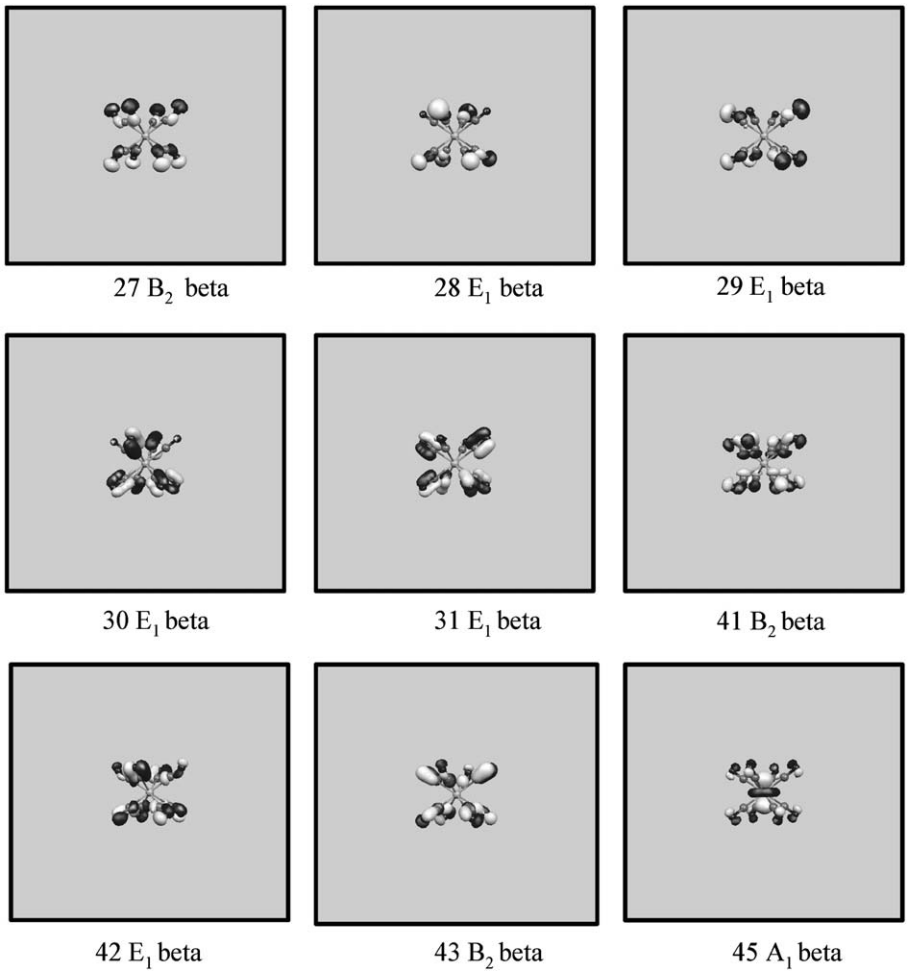

Fig. 3. Active molecular orbitals of the $[Re(CN)_8]^{2-}$ complex.

in a PCM using the time-dependent perturbation theory approach (TD-DFT) [23,24]. The allowed spin singlet transition for these complexes were calculated based on the ground state structures of the square antiprismatic model. The objective was to evaluate the electronic structure of the excited states by direct electronic excitations. Only singlet–singlet transitions were considered in these TD-DFT–PCM scalar relativistic calculations. The calculated transitions are shown in Table 4. Here, we considered as permitted or allowed transitions those whose oscillator strengths are non-zero. The molecular orbitals which are active in the electronic transitions are depicted in Figs. 2 and 3.

3.4. $[Re(CN)_8]^{-3}$

The electronic absorption spectra of $(Bu_4N)_3[Re(CN)_8]$ in acetonitrile is remarkably similar to the spectra of the isoelectronic $[M(CN)_8]^{4-}$ $(M = Mo, W)$ complexes, suggesting that $[Re(CN)_8]^{3-}$ may convert to a dodecahedral geometry (D_{2d}) in solution [5,8,9]. This complex shows an experimental absorption spectrum with bands centered at (196 nm ($\varepsilon_M = 13\,200$), 231(sh), 252 (sh), 298 ($\varepsilon_M = 168$), 348 ($\varepsilon_M = 76$), 436 ($\varepsilon_M = 22$)). Accordingly, the three bands with larger wavelengths and small extinction coefficients were assigned as spin-allowed d–d transitions [5]. Although, our calculations based on the square antiprismatic model are able to find these d–d bands, these are calculated with oscillator strength values equal to zero with no intense transitions, as can be seen from Table 4-A. The calculated excitation at 202.9 nm could be related with the experimental band centered at 196 nm. This band involves the ligands (CN^-) and the metal (Re). This transition shows three principal components: (i) LMCT: the component with greater weight (43%) corresponds to $37E_2(\pi) \rightarrow 46E_2(d_{x^2-y^2})$, (ii) LMCT: the second component (27.9%) corresponds to a $36E_2(\pi) \rightarrow 47E_2(d_{xy})$ transition; (iii)MMCT: the last component (22.8%) corresponds to $45A_1(d_{z^2}) \rightarrow 53B_2(p_z)$ transition. The active molecular orbitals involved in these transitions are depicted in Fig. 2. Thus, our oscillator strength calculated values equal to zero suggest that the $[Re(CN)_8]^{-3}$ complex in solution may distort toward the dodecahedral structure (D_{2d}), since under this geometry the oscillator strengths are non-zero.

3.5. $[Re(CN)_8]^{-2}$

There are not reported measurements of the electronic spectrum of this system. Thus, our results reported here

have predictive character. The theoretical calculations in acetonitrile are summarized in Table 4-B. We can observe that the excitations are displaced at very high wavelengths with significant oscillator strength values, granting a strong luminescent character. The emission could be described through a LMCT excited state [35]. The band at 427.9 nm is the most intensive ($f = 0.0373$), and it is doubly degenerated. It is composed by a transition of the LMCT type: $30E_1(\pi) \rightarrow 45A_1(d_{z^2})$ and $31E_1(\pi) \rightarrow 45A_1(d_{z^2})$, which can be visualized from the active molecular orbitals shown in Fig. 3.

4. Conclusions

We reported here scalar and four component relativistic density functional calculations on each of the title compounds. We found that lowest excited state of each complex split by spin–orbit interaction by about 0.5 eV. The calculated molecular electronegativities χ indicate that the open-shell complex is less reactive than the closed shell complex. The large deviation of the molecular g tensor components from the spin-only value arises from the effects of spin–orbit coupling affecting the LUMO and HOMO-1 orbitals of $[Re(CN)_8]^{2-}$. The calculated optical electronic transitions for both complexes in a polarizable continuum model using a time dependent density functional (TDDFT)/B3LYP formalism indicates that may occur a distortion toward dodecahedral geometry in solution. Our calculated values of the LMCT transitions and the oscillator strengths of $[Re(CN)_8]^{2-}$ suggest that this anion could be luminescent.

Acknowledgement

This work has been supported in part by Fondecyt. 1030148, Fondecyt 1020141, UNAB-DI 12-04, UNAB-DI 20-04 and the Millennium Nucleus of Applied Quantum Mechanics and Computational Chemistry, P02-004-F.

References

[1] K.R. Dunbar, R.A. Heintz, Prog. Inorg. Chem. 45 (1997) 283.
[2] L. Yet, Angew. Chem. Int. Ed. Engl. 40 (2001) 875.
[3] O. Kahn, C.J. Martinez, Science 279 (1998) 44.
[4] L.M.C. Beltran, J.R. Long, Acc. Chem. Res. 38 (2005) 325.
[5] M.V. Bennett, J.R. Long, J. Am. Chem. Soc. 125 (2003) 2394.
[6] J.R. Perumaredi, A.D. Lierh, W.A. Adamson, J. Am. Chem. Soc. 85 (1963) 249.
[7] W.P. Griffith, P.M. Kiernan, J.M. Bregault, J. Chem. Soc. Dalton Trans. (1978) 1411.
[8] M.F.A. Hendrickx, V.S. Mironov, L.F. Chitobaru, A. Ceulemans, Inorg. Chem. 42 (2003) 590.
[9] M.F.A. Hendrickx, V.S. Mironov, L.F. Chitobaru, A. Ceulemans, Inorg. Chem. 43 (2004) 3142.
[10] Amsterdam Density Functional (ADF) code, release 2004, Vrije Universiteit, Amsterdam, The Netherlands.
[11] E.J. Baerends, D.E. Ellis, P. Ros, Chem. Phys. 2 (1973) 41.
[12] P.M. Boerrigter, G. te Velde, E.J. Baerends, Int. J. Quantum Chem. 33 (1998) 87.
[13] G. te Velde, F.M. Bickelhaupt, S.J.A. Van Gisbergen, C. Fonseca Guerra, E.J. Baerends, J.G. Snijders, T.J. Ziegler, Comput. Chem. 22 (2001) 931.
[14] A.D. Becke, Phys. Rev. A. 38 (1988) 3098.
[15] J.P. Perdew, Phys. Rev. B. 33 (1986) 8822.
[16] J.P. Perdew, Phys. Rev. B. 34 (1986) 7046.
[17] M. Cossi, V. Barone, J. Phys. Chem. A 102 (1998) 1995.
[18] S. Miertus, E. Scrocco, J. Tomasi, Chem. Phys. 55 (1981) 117.
[19] M. Cossi, V. Barone, R. Cammi, J. Tomasi, Chem. Phys. Lett. 255 (1996) 327.
[20] M.J. Frisch et al., GAUSSIAN 98 rev. A.11, Inc., Pittsburg, PA, 2002.
[21] D. Andrae, U. Hausserman, M. Dolg, H. Stoll, H. Preuss, Theor. Chim. Acta 77 (1990) 123.
[22] A. Bergner, M. Dolg, W. Kuchle, H. Stoll, H. Preuss, Mol. Phys. 80 (1993) 1431.
[23] R. Bauernschmitt, R. Ahlrichs, Chem. Phys. Lett. 256 (1996) 454.
[24] M.E. Casida, C. Jamorski, K.C. Casida, D.R. Salahub, J. Chem. Phys. 108 (1998) 4439.
[25] C.Y. Yang, D.A. Case, in: J.P. Dahl, J. Avery (Eds.), Local Density Approximations in Quantum Chemistry and Solid State Physics, Plenum, New York, 1983.
[26] R. Arratia-Pérez, L. Hernández-Acevedo, J. Chem. Phys. 110 (1999) 2529.
[27] L. Vera, F. Zuloaga, J. Phys. Chem. 88 (1984) 6415.
[28] L. Alvarez-Thon, L. Hernández-Acevedo, R. Arratia-Perez, J. Chem. Phys. 115 (2001) 726.
[29] R. Arratia-Pérez, L. Hernández-Acevedo, J. Chem. Phys. 118 (2003) 7425.
[30] R. Arratia-Pérez, L. Hernández-Acevedo, G.L. Malli, J. Chem. Phys. 121 (2004) 7743.
[31] A.H. MacDonald, S.H. Vosko, J. Phys. C 12 (1979) 2977.
[32] A.K. Rajagopal, J. Phys. C 11 (1978) L943;
A.K. Rajagopal, Adv. Chem. Phys. 41 (1980) 59.
[33] J.E. Harriman, Theoretical Foundations of Electron Spin Resonance, Academic Press, New York, 1978.
[34] W. Weltner Jr., Magnetic Atoms and Molecules, Dover, New York, 1989.
[35] Y. Foo, J.R. Kirchhoff, J. Am. Chem. Soc. 116 (1994) 3599.